Journal of Applied Science and Engineering, Vol. 21, No. 2, pp. 205–212 (2018) *DOI: 10.6180/jase.201806_21(2).0008*

Numerical Simulation of the Supersonic Base Flows with Emphasis on Turbulence Model

Chang-Fei Zhuo[1]*, Yan-Bing Zou[1,2] and Peng Xu[3]

[1]*School of Mechanical Engineering, Nanjing University of Science and Technology, Nanjing 210094, P.R. China*
[2]*Wuhan Guide Infrared Co., Ltd, Wuhan 430040, P.R. China*
[3]*The Technical Center of Jinxi Industries Group Co., Ltd, Taiyuan 030027, P.R. China*

Abstract

Numerical investigations of the supersonic flow over a base of cylinder using Reynolds averaged Navier-Stokes (RANS) method have been performed in detail in this paper. The flow is along a cylinder axis and separates suddenly at a blunt base corner. The performance of several turbulence models have been examined in this study. They include: *Spalart-Allmaras* (*S-A*), *k*-ω, *k*-ω BSL, and *k*-ω SST. Some important statistics computed for engineering in the wake region of the flow are compared with the experimental results for the same conditions and configurations. For *k*-ω SST turbulence model, the performance of three compressibility models are examined. In addition, the performance of numerical scheme for spatial discretization is examined for the supersonic base flow. In general, *k*-ω SST and *k*-ω BSL turbulence model perform better in the near wake than *S-A* and *k*-ω model, and predict the base pressure and axial length of the recirculation bubble much better. Three compressibility models for *k*-ω SST turbulence model perform much more different, and over-predict or under-predict the base pressure. From the numerical scheme point of view, AUSMPW+ scheme is more suitable for the numerical calculation of the base flow field about the supersonic flows.

Key Words: Computational Fluid Dynamics, Turbulence Model, Base Flow, Compressible Modification, Numerical Scheme

1. Introduction

Supersonic flows past an axisymmetric base are fundamental and important for many engineering problems [1]. For instance, reusable launch vehicles, especially vertical take-off and landing type vehicles with maneuvering at a certain speed range, have large base area. Their aerodynamic characteristics are strongly influenced by the base flow field in their flight path. Therefore, accurate estimation of the base flow field and the applied force acting on the base are an important issues for the design of such vehicles.

Supersonic base flows is in the region where turbulence plays an important role [2]. So numerical simulation reveals to be an appropriate prediction tool though it is difficult to numerically simulate this complex physical phenomena. Some previous studies [3,4] of base flows applied the algebraic turbulence models of *Baldwin-Lomax* [5] to eliminate the complexity of numerical and physical modeling. Several investigations [6–8] have incorporated *k*-ε two-equation turbulence models and *Algebraic Stress Model* (*ASM*) and obtained a better agreement with experimental data. The *k*-ε two-equation and its similar models couldn't predict the size of the recirculating region, therefore the disagreements between the mean velocity profiles and turbulent stresses were still existence. Soo [9] presented an improvement to the *k*-ε turbulence model and examined the effects of

*Corresponding author. E-mail: njust203zcf@126.com

compressibility and non-equilibrium modifications for k-ε turbulence models. Franck [10] investigated the influence of four simple corrections of the *Spalart-Allmaras* model in order to better predict the supersonic base flows, but they highlighted the turbulence modeling's shortcomings in predicting levels of the experimental base pressure.

This paper describe the computational investigation of the supersonic base flows for the same experimental model and conditions. The paper are organized as follows. First, several turbulence models have been examined for the supersonic base flows in this study. They include: *Spalart-Allmaras*, k-ω, k-ω BSL, and k-ω SST. Then, for k-ω SST turbulence model, compressibility is also investigated. Finally, the performance of spatial discretization schemes are examined for the supersonic base flows.

2. Mathematical Method

2.1 Governing Equations

The Reynolds-averaged Navier-stokes equations can be written in the following form [9]:

$$\frac{\partial \boldsymbol{U}}{\partial t}+\frac{\partial(\boldsymbol{F}_j-\boldsymbol{Fv}_j)}{\partial x_j}=0 \tag{1}$$

where $\boldsymbol{U}$ is the conservative fluxes, $\boldsymbol{F}$ is convection fluxes and $\boldsymbol{Fv}$ is viscous fluxes.

2.2 Turbulence Model

The *Spalart-Allmaras* model [11] (Called *S-A* model) is given by the following equation:

$$\begin{aligned}\frac{\partial \rho\tilde{\nu}}{\partial t}+\frac{\partial \rho u_i\tilde{\nu}}{\partial x_i}&=c_{b1}\tilde{S}\rho\tilde{\nu}+\frac{1}{\sigma}(\nabla(\mu+\rho\tilde{\nu})\nabla\tilde{\nu}+c_{b2}\rho(\nabla\tilde{\nu})^2)\\&-\rho c_{w1}f_w\left(\frac{\tilde{\nu}}{d}\right)^2\end{aligned} \tag{2}$$

and the eddy viscosity is computed from:

$$\nu_t=\tilde{\nu}f_{v1} \tag{3}$$

The k-ω model [12] is given by the following equation:

$$\begin{cases}\dfrac{\partial\rho k}{\partial t}+\dfrac{\partial}{\partial x_i}\left(\rho u_i k-(\mu+\sigma_k\mu_t)\dfrac{\partial k}{\partial x_i}\right)=\tau_{ij}S_{ij}-\beta^*\rho\omega k\\ \dfrac{\partial\rho\omega}{\partial t}+\dfrac{\partial}{\partial x_i}\left(\rho u_i w-(\mu+\sigma_w\mu_t)\dfrac{\partial w}{\partial x_i}\right)=\alpha\dfrac{\omega}{k}\tau_{ij}S_{ij}-\beta\rho\omega^2\end{cases} \tag{4}$$

and the eddy viscosity is computed from:

$$\nu_t=\frac{k}{\omega} \tag{5}$$

The k-ω SST model [13] is given by the following equation:

$$\begin{cases}\dfrac{\partial\rho k}{\partial t}+\dfrac{\partial}{\partial x_i}\left(\rho u_i k-(\mu+\sigma_k\mu_t)\dfrac{\partial k}{\partial x_i}\right)=P_k-\beta^*\rho\omega k\\ \dfrac{\partial\rho\omega}{\partial t}+\dfrac{\partial}{\partial x_i}\left(\rho u_i w-(\mu+\sigma_w\mu_t)\dfrac{\partial w}{\partial x_i}\right)=P_\omega-\beta\rho\omega^2+2(1-F_1)\Gamma\end{cases} \tag{6}$$

and the eddy viscosity is computed from:

$$\nu_t=\frac{a_1 k}{\max(a_1\omega,\Omega F_2)} \tag{7}$$

Considering the compressibility correction, the compressibility correction k-ω SST model is given by the following equation:

$$\begin{cases}\dfrac{\partial\rho k}{\partial t}+\dfrac{\partial}{\partial x_i}\left(\rho u_i k-(\mu+\sigma_k\mu_t)\dfrac{\partial k}{\partial x_i}\right)\\ \quad=P_k-\beta_n^*\rho\omega k+\prod_{c1}+\prod_{c2}\\ \dfrac{\partial\rho\omega}{\partial t}+\dfrac{\partial}{\partial x_i}\left(\rho u_i w-(\mu+\sigma_w\mu_t)\dfrac{\partial w}{\partial x_i}\right)\\ \quad=P_\omega-\beta_n\rho\omega^2+2(1-F_1)\Gamma\end{cases} \tag{8}$$

where the correction term are given by [12,14]:

$$\begin{cases}\prod_{c1}=-\sigma_c\dfrac{\mu_t}{\rho^2}\dfrac{\partial\rho}{\partial x_j}\dfrac{\partial p}{\partial x_j},\quad \sigma_c=0.006\\ \prod_{c2}=\alpha_2 P_k M_t+\alpha_3\rho\varepsilon M_t^2,\ \alpha_2=-0.15,\ \alpha_3=0.2\end{cases} \tag{9}$$

where the correction parameter are given by [12]:

$$\begin{cases}\beta_n^*=\beta^*\left[1+\xi^*F(M_t)\right]\\ \beta_n=\beta-\beta^*\xi^*F(M_t)\end{cases} \tag{10}$$

For the correction model of Sarkar [15] (Called *k*-ω SST-CC1), the additional functions are given by:

$$\xi^* = 1,\ F(M_t) = M_t^2 \qquad (11)$$

For the correction model of Zeman [16] (Called *k*-ω SST-CC2), the additional functions are given by:

$$F(M_t) = \left[1 - e^{-\frac{(\gamma+1)(M_t - M_{t0})^2}{2\Lambda^2}}\right] H(M_t - M_{t0}) \qquad (12)$$

where $H(x)$ is unit step function, $\xi^* = 0.75$, $\Lambda = 0.66$, $M_{t0} = 0.25\sqrt{2/(\gamma+1)}$, γ is specific heat ratio.

For the correction model of Wilcox [12] (Called *k*-ω SST-CC3), the additional functions are given by:

$$\begin{cases} \xi^* = 2,\ M_{t0} = 0.25 \\ F(M_t) = (M_t^2 - M_{t0}^2) H(M_t - M_{t0}) \end{cases} \qquad (13)$$

The governing equation and parameter of *k*-ω BSL model [17] are consistent with *k*-ω SST model, and only the eddy viscosity is different. The eddy viscosity for *k*-ω BSL model is computed from:

$$\nu_t = \frac{k}{\omega} \qquad (14)$$

2.3 Numerical Scheme

In order to improve the accuracy of spatial discretization, we should reconstruct the primitive variables before computing the convection flux quantities of the governing equation using upwind scheme.

In the computational domain, NND scheme [18] is used. In the variable interpolation approach, extrapolated values for left and right sides of the interface between cells are calculated as below:

$$\begin{cases} W_L = W_I + \frac{1}{2}\min\mathrm{mod}(W_{I+1} - W_I, W_I - W_{I-1}) \\ W_R = W_{I+1} - \frac{1}{2}\min\mathrm{mod}(W_{I+1} - W_I, W_{I+2} - W_{I+1}) \end{cases} \qquad (15)$$

where W_L, W_R are the state primitive variables (ρ, u_i, p) to the left and right of the interface between cell I and cell I+1. The limiter function min mod is given by:

$$\min\mathrm{mod}(x, y) = [Sign(x) + Sign(y)]\min(|x|, |y|) \qquad (16)$$

The Steger-warming scheme [19], Van-Leer [20], HLLC scheme [21], AUSMPW+ scheme [22] and AUSMDV scheme [23] are used to compute the convection fluxes, respectively.

3. Numerical Results and Discussions

The supersonic base flows at Mach number 2.46 experimentally investigated by Herrin [24] is used as reference for the present study.

The mesh used for the base flow calculations is presented in Figure 1. Mach number, density, pressure, temperature, Reynolds number and the cylindrical radius (R) in the far field are 2.46, 0.7549 kg/m^3, 31415.0 Pa, 145.0 K, 4.5 × 10^7 m^{-1} and 31.75 mm, respectively. The domain size is 12R downstream the base and 4.8R in the radial direction. The cylinder length is equal to 3R and corresponds to the extent necessary to the boundary layer to develop in order to match the experimental height at the base. The grid density is approximatively 1620000 points with 36 points in the azimuthal direction due to the zero incidence case.

The contours of the main flow parameters behind the base for different turbulence models are shown in Figure 2~Figure 5. As seen from the Mach number contour, the shape of the recirculation bubble predicted by *k*-ω SST is nearly consistent with the results predicted by *k*-ω BSL. The axial length of the recirculation bubble predicted by *S-A* is very small. The axial length of the recirculation bubble predicted by *k*-ω is much longer than the results predicted by *k*-ω SST and *k*-ω BSL, and the recirculation bubble is relatively oblate. Moreover, the width of the base wake (The distance between the up and down slip

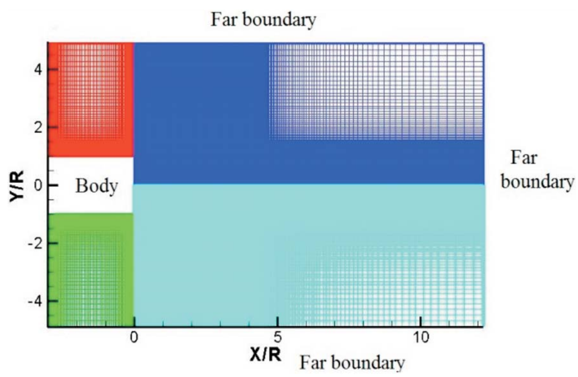

Figure 1. 2D computational mesh in the *x*-*y* plan.

lines in base wake) zone predicted by *k*-ω is much less than the results predicted by *k*-ω SST and *k*-ω BSL. The boundary of the base wake zone predicted by *S-A* is vague, but the width of the zone is much greater than the results predicted by the other models. As can be seen from the turbulent variable contour, the distributions of the turbulent kinetic energy *k* predicted by *k*-ω SST, *k*-ω BSL and *k*-ω are nearly consistent, and the maximum value of the turbulent kinetic energy *k* exists near the secondary compression zone of the free stream. However, the turbulent kinetic energy *k* predicted by *k*-ω is much lower than the counterparts by *k*-ω SST and *k*-ω BSL, as well as the eddy viscosity radio. The maximum value of turbulent variables ν predicted by *S-A* distributes in the recirculation zone, and the eddy viscosity ratio in the base wake is much larger than the results predicted by *k*-ω SST and *k*-ω BSL. Exactly, the maximum of the eddy viscosity ratio in the base wake calculated by *k*-ω model is proximately twice of the results predicted by *k*-ω SST and *k*-ω BSL.

From the engineering point of view, average base pressure is the most important parameter. Figure 6 shows the pressure distributions along the base under different turbulence models. The simulations by *k*-ω SST and *k*-ω BSL are mainly in accordance with each other. The trend of the simulation by *k*-ω coincides with the counterpart of *k*-ω SST, but the numerical results by *k*-ω is higher than the results by *k*-ω SST. The tendency of the simulation by *S-A* is the same as the case of the simulation by *k*-ω SST, but the numerical results by *S-A* is lower than

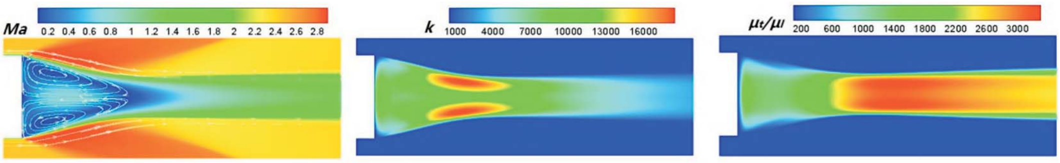

(a) Mach number (b) Turbulent variables (*k*) (c) Eddy viscosity radio

Figure 2. The contours behind the base for the simulation by *k*-ω SST.

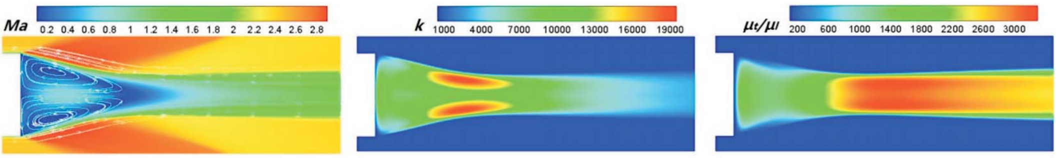

(a) Mach number (b) Turbulent variables (*k*) (c) Eddy viscosity radio

Figure 3. The contours behind the base for the simulation by *k*-ω BSL.

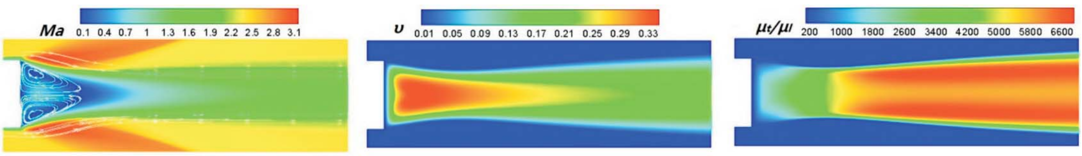

(a) Mach number (b) Turbulent variables (*v*) (c) Eddy viscosity radio

Figure 4. The contours behind the base for the simulation by *S-A*.

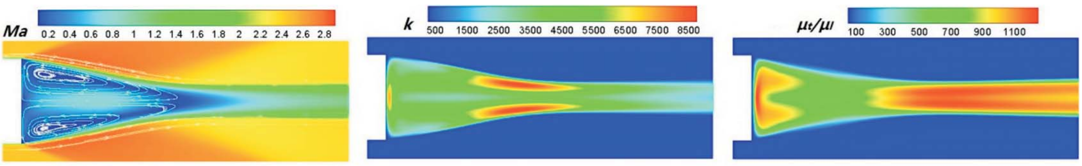

(a) Mach number (b) Turbulent variables (*k*) (c) Eddy viscosity radio

Figure 5. The contours behind the base for the simulation by *k*-ω.

experimental results. However, in contrast to the near-constant experimental data, the base pressure which are predicted by all the models show relatively large variations in magnitude along the base.

The velocity profile along the centerline of the cylinder wake under different turbulence models are shown in Figure 6. *S-A* greatly underestimates the shear layer reattachment location. *k*-ω greatly overestimates the shear layer reattachment location. However, *k*-ω SST predicts the location of the shear layer reattachment reasonably as well as *k*-ω BSL and it is in good accordance with experimental results. The peak reverse velocity is overestimated by all the models, which helps explain the increased variation in pressure along the base. Streamlines flowing along the centerline towards the base stagnate in the center of the base, leading to the high pressure seen there. In addition, all the turbulence models fail to predict the maximum backflow velocity position.

The base flows is simulated by an original *k*-ω SST turbulence model and three compressible correction *k*-ω SST models, and the results of the calculation are shown in Figure 7~Figure 9. As can be seen from the Mach number contour, the shape of the recirculation bubble predicted by *k*-ω SST-CC1 and *k*-ω SST-CC2 are relatively large ,which are similar to the results predicted by *k*-ω in Figure 5. The volume and axial length of the recirculation bubble predicted by *k*-ω SST-CC2 is small compared to the results predicted by *k*-ω SST-CC1 and *k*-ω SST-CC3. Simultaneously, the width of the base wake zone predicted by *k*-ω SST-CC2 is much larger than the results predicted by *k*-ω SST-CC1 and *k*-ω SST-CC3. As can be seen from the turbulent variable contour, the distribution of both the turbulent kinetic energy *k* and the eddy viscosity radio predicted by *k*-ω SST-CC1 is nearly

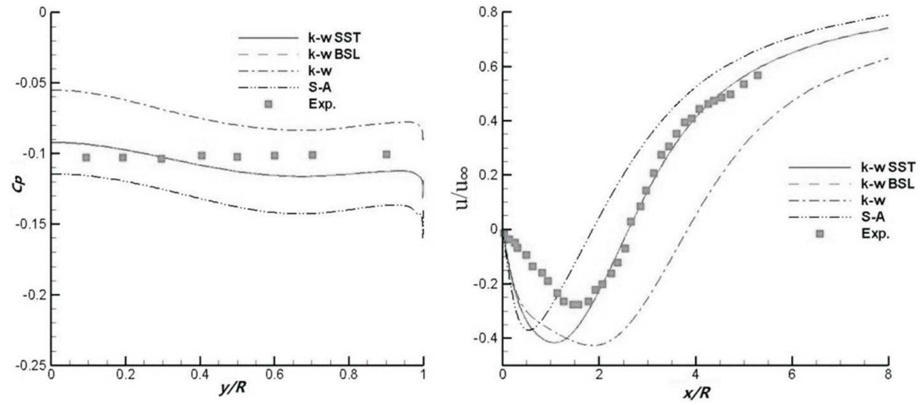

Figure 6. Base pressure coefficient along radial position and velocity (normalized by freestream velocity) along the centerline of the cylinder wake under different turbulence models.

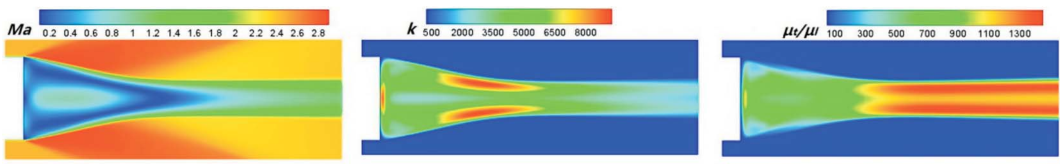

(a) Mach number (b) Turbulent variables (*k*) (c) Eddy viscosity radio

Figure 7. The contours behind the base for the simulation by *k*-ω SST-CC1.

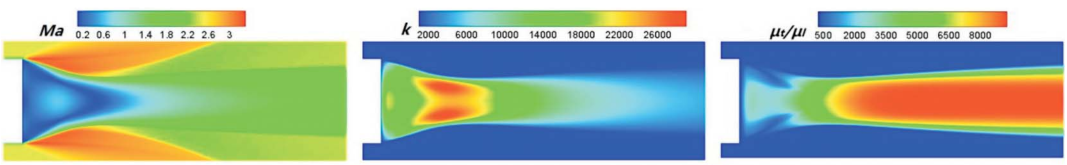

(a) Mach number (b) Turbulent variables (*k*) (c) Eddy viscosity radio

Figure 8. The contours behind the base for the simulation by *k*-ω SST-CC2.

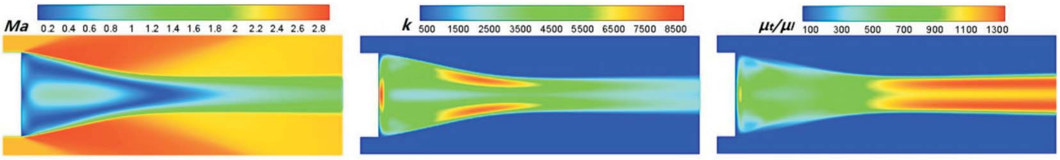

(a) Mach number (b) Turbulent variables (k) (c) Eddy viscosity radio

Figure 9. The contours behind the base for the simulation by k-ω SST-CC3.

consistent with the results predicted by k-ω SST-CC3. Both the turbulent kinetic energy k and the eddy viscosity predicted by k-ω SST-CC1 and k-ω SST-CC3 are much lower than the counterparts of k-ω SST calculations. However, the turbulent kinetic energy k and the eddy viscosity predicted by k-ω SST-CC2 in the base wake are much larger than the results predicted by k-ω SST, k-ω SST-CC1 and k-ω SST-CC3.

The velocity profiles along the centerline of the cylinder wake under different compressibility correction k-ω SST turbulence models are shown in Figure 10. Combined with the main flow parameter contours, the reattachment point predicted by k-ω SST-CC2 is located at nearly X/R = 1.8, which is underpredicted by about 33.3% comparing to the experimental value of X/R = 2.7. The reattachment point predicted by k-ω SST-CC1 and k-ω SST-CC3 is located at nearly X/R = 3.5, which is overpredicted by about 29.3% comparing to the experimental value of X/R = 2.7. In addition, all the compressibility correction models fail to predict the position and intensity of the maximum backflow velocity. However, the maximum backflow velocity predicted by k-ω SST-CC1 and k-ω SST-CC3 is much larger than the results predicted by k-ω SST, but the maximum backflow velocity predicted by k-ω SST-CC2 is much lower than the results predicted by k-ω SST. In a word, k-ω SST-CC1 and k-ω SST-CC3 reduce the levels of eddy viscosity, and increases the volume and velocity of the recirculation region. Inversely, k-ω SST-CC2 increases the levels of eddy viscosity, reducing the size of the recirculation region and the peak reverse velocity.

Figure 10 also show the pressure distributions along radial position under different compressibility correction k-ω SST turbulence models. As can be seen, the tendency of pressure coefficient distributions predicted by k-ω SST-CC2 is consistent with the tendency predicted by k-ω SST, while the values predicted by both k-ω SST-CC2 and k-ω SST are much lower than the experimental values. The results predicted by k-ω SST-CC1 and k-ω SST-CC3 have much larger variations in the magnitude of the pressure coefficient than other models along radial position. In the area of $Y/R < 0.3$, the pressure coefficient distributions predicted by k-ω SST-CC1 and k-ω SST-CC3 are significantly different. In the area of $Y/R > 0.3$, the pressure coefficient distributions predicted by k-ω SST-CC1 is consistent with the results predicted by k-ω SST-CC2.

The calculations predicted by k-ω SST, k-ω SST-CC1,

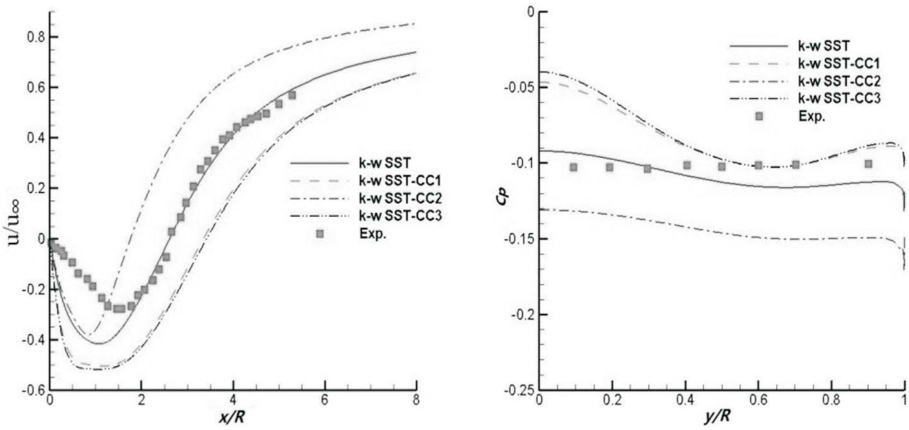

Figure 10. Velocity along the centerline of the cylinder wake and base pressure coefficient along radial position considering the compressibility correction.

k-ω SST-CC2 and *k*-ω SST-CC3 are quite different. For instance, the recirculation sizes they estimate are too big or too small, leading to the pressure coefficient distribution in the base plane quite different with experimental value. However, the compressibility correction has a great impact on the numerical results on base flows in the supersonic flows. So, from the point of compressibility correction, in order to make *k*-ω SST model more suitable for the numerical simulation of the complex supersonic base flows, correcting *k*-ω SST model will be carried out in future.

The results predicted by various numerical schemes (Steger-warming, Van-leer, HLLC, AUSMPW+, AUSMDV) are shown in Figure 11. Both the pressure coefficient distributions and velocity distributions calculated by all numerical schemes are nearly consistent with another, indicating that the numerical schemes don't have much impact on the flow filed calculation under the conditions in this paper. Therefore, there is no need to show the contours of the main flow parameters behind the base for different numerical schemes, and it is similar to the results shown in Figure 2. However, from detail view, the maximum velocity calculated by using AUSMPW+ scheme is smaller than other numerical schemes, and the position of the maximum velocity is closer to the experimental result. Meanwhile, as can be seen from the pressure coefficient distribution, the pressure coefficient distribution calculated by using AUSMPW+ scheme is larger than the counterparts of other numerical schemes, and it is closer to the experimental value. Therefore, it can be concluded that the AUSMPW+ scheme is more suitable for the numerical calculation for the base flows field in the supersonic flows.

4. Conclusions

The performance of several turbulence models are examined for supersonic base flows in this paper, including: *Spalart-Allmaras* (*S-A*), *k*-ω, *k*-ω BSL, and *k*-ω SST. Computed some important statistics for engineering in the wake region of the flow are compared with experimental results for the same conditions and configurations. *k*-ω SST and *k*-ω BSL turbulence model perform better in the near wake than *S-A* and *k*-ω model, and predict the base pressure and axial length of the recirculation bubble much better. For *k*-ω SST turbulence model, the performance of three compressibility models are examined. Three compressibility models for *k*-ω SST turbulence model perform a much difference, and they overpredict or underpredict the base pressure. In addition, the performance of numerical schemes for spatial discretization are examined for the supersonic base flows. From the numerical scheme point of view, AUSMPW+ scheme is more suitable for the numerical calculation for the base flow field in the supersonic flow.

Acknowledgments

This work has been financially supported by the National Natural Science Foundation of China (Grant No. 11602109), and the Jiangsu Province Natural Science Foundation of China (No. BK20160836).

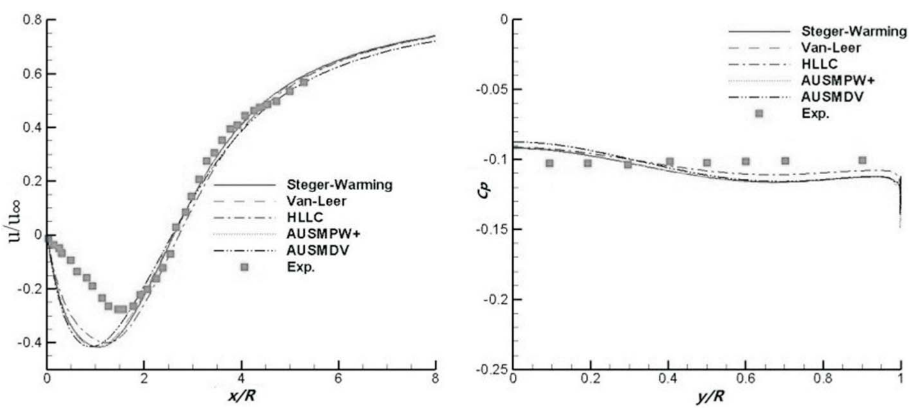

Figure 11. Velocity along the centerline of the cylinder wake and base pressure coefficient along radial position under different numerical schemes.

References

[1] Soshi, K. and Kozo, F., "Computational Study of a Supersonic Base Flow Using LES/RANS Hybrid Methodology," AIAA Paper 2004-68 (2004). doi: 10.2514/6.20 04-68

[2] Sahu, J. and Heavey, K. R., "Numerical Investigation of Supersonic Base Flow with Base Bleed," AIAA Paper 95-3459 (1995). doi: 10.2514/2.3173

[3] William, B. C., Khaled, S. A. and William, K. A., "Comparison of Algebraic Turbulence Models for Afterbody Flows with Jet Exhaust," *AIAA Journal*, Vol. 30, pp. 2716–2722 (1992). doi: 10.2514/3.11289

[4] Yang, A. S., Hsieh, W. H. and Kuo, K. K., "Theoretic Study of Supersonic Flow Separation over a Rearward-facing Step," AIAA Paper 91-2161 (1991). doi: 10.2514/2.7642

[5] Baldwin, B. C. and Lomax, H., "Thin Layer Approximation and Algebraic Model for Separated Turbulent Flows," AIAA Paper 78-257 (1978). doi: 10.2514/6.1978-257

[6] Nichols, R. H., Maus, J. R., Spinetti, R. L. and Movlvik, G. A., "Calculation of High Speed Base Flows," AIAA Paper 92-2679 (1992). doi: 10.2514/6.1992-2679

[7] Lin, H. and Chieng, C. C., "Comparisons of TVD Schemes for Turbulent Transonic Projectile Aerodynamics Computations with a Two-equation Model of Turbulence," *International Journal for Numerical Methods in Fluids*, Vol. 16, pp. 365–390 (1993). doi: 10.1002/fld.1650160503

[8] Chuang, C. C. and Chieng, C. C., "Transonic Turbulent Separated Flow Predictions Using a Two Layer Turbulence Model," *AIAA Journal*, Vol. 31, No. 5, pp. 816–817 (1993). doi: 10.2514/3.11689

[9] Soo, H. P., Sumanta, A. and Jang, H. K., "An Improved Formulation of k-ε Turbulence Models for Supersonic Base Flow," AIAA Paper 2005-4707 (2005). doi: 10.2514/6.2005-4707

[10] Franck, S., Sebastien, D. and Philippe, G., "Numerical Simulations of Projectile Base Flow," AIAA Paper 2006-1116 (2006). doi: 10.2514/6.2006-1116

[11] Spalart, P. R. and Allmaras, S. R., "A One-equation Turbulence Model for Aerodynamics Flows," AIAA Paper 92-0439 (1992). doi: 10.2514/6.1992-439

[12] Wilcox, D. C., *Turbulence Modeling for CFD*, Califomia: DCW Industries Inc., pp. 243–261 (2006).

[13] Menter, F. R., "Two Equation Eddy Viscosity Turbulence Models for Engineering Applications," *AIAA Journal*, Vol. 32, No. 8, pp. 1598–1605 (1994). doi: 10.2514/3.12149

[14] Sarkar, S., "The Pressure-dilatation Correlation in Compressible Flows," *Physics of Fluids*, Vol. 4, pp. 2674–2682 (1992). doi: 10.1063/1.858454

[15] Sarker, S., Erlebacher, G. and Hussaini, M. Y., "The Analysis and Modeling of Dilatational Terms in Compressible Turbulence," *Journal of Fluid Mechanics*, Vol. 227, pp. 473–493 (1991). doi: 10.1017/S0022112091000204

[16] Zeman, O., "Dilatational Dissipation: the Concept and Application in Modeling Compressible Mixing Layers," *Physics of Fluids A Fluid Dynamics*, Vol. 2, pp. 178–188 (1990). doi: 10.1063/1.857767

[17] Menter, F. R., "Improved Two-equation k-ω Turbulence Models for Aerodynamic Flows," NASA TM-103975 (1992).

[18] Zhang, H. X., Chen, J. Q. and Gao, S. C., "Numerical Simulation of Supersonic Non-equilibrium Flows for H_2/O_2 Combustion," *Journal of Astronautics*, Vol. 15, pp. 14–23 (1994).

[19] Steger, J. L. and Warming, R. F., "Flux Vector Splitting of the Invisid Gas-dynamics Equations with Application to Finite Difference Methods," *Journal of Computational Physics*, Vol. 40, pp. 263–293 (1981). doi: 10.1016/0021-9991(81)90210-2

[20] Van, Leer. B., "Flux Vector Splitting for Euler Equations," *Lecture Notes in Physics*, pp. 170:507–512 (1982).

[21] Toro, E. F., *Riemann Solvers and Numerical Methods for Fluid Dynamics*, Springer, Berlin (1997). doi: 10.1007/978-3-662-03490-3

[22] Kim, K. H., Kim, C. and Rho, O. H., "Methods for the Accurate Computations of Hypersonic Flows: I. AUSMPW+ Scheme," *Journal of Computational Physics*, Vol. 174, pp. 38–80 (2001). doi: 10.1006/jcph.2001.6873

[23] Yasuhiro, W. and Liu, M. S., "A Flux Splitting Scheme with High-resolution and Robustness for Discontinuities," AIAA Paper 94-0083 (1994). doi: 10.2514/6.1994-83

[24] Herrin, J. L. and Dutton, J. C., "Supersonic Base Flow Experiments in the Near-wake of a Cylindrical Afterbody," AIAA Paper 93-2924 (1993). doi: 10.2514/3.11953

Manuscript Received: Mar. 29, 2017

Accepted: Feb. 6, 2018